Published in final edited form as:
J Immunol. 2009 September 1; 183(5): 3040–3052. doi:10.4049/jimmunol.0900562.

Inhibition of Thymic Adipogenesis by Caloric Restriction Is Coupled with Reduction in Age-Related Thymic Involution[1]

Hyunwon Yang, **Yun-Hee Youm**, and **Vishwa Deep Dixit**[2]
Laboratory of Neuroendocrine-Immunology, Pennington Biomedical Research Center, Louisiana State University System, Baton Rouge, LA 70808

Abstract

Aging of thymus is characterized by reduction in naive T cell output together with progressive replacement of lymphostromal thymic zones with adipocytes. Determining how calorie restriction (CR), a prolongevity metabolic intervention, regulates thymic aging may allow identification of relevant mechanisms to prevent immunosenescence. Using a mouse model of chronic CR, we found that a reduction in age-related thymic adipogenic mechanism is coupled with maintenance of thymic function. The CR increased cellular density in the thymic cortex and medulla and preserved the epithelial signatures. Interestingly, CR prevented the age-related increase in epithelial-mesenchymal transition (EMT) regulators, FoxC2, and fibroblast-specific protein-1 (FSP-1), together with reduction in lipid-laden thymic fibroblasts. Additionally, CR specifically blocked the age-related elevation of thymic proadipogenic master regulator, peroxisome proliferator activated receptor γ (PPARγ), and its upstream activator xanthine-oxidoreductase (XOR). Furthermore, we found that specific inhibition of PPARγ in thymic stromal cells prevented their adipogenic transformation in an XOR-dependent mechanism. Activation of PPARγ-driven adipogenesis in OP9-DL1 stromal cells compromised their ability to support T cell development. Conversely, CR-induced reduction in EMT and thymic adipogenesis were coupled with elevated thymic output. Compared with 26-mo-old ad libitum fed mice, the T cells derived from age-matched CR animals displayed greater proliferation and higher IL-2 expression. Furthermore, CR prevented the deterioration of the peripheral TCR repertoire diversity in older animals. Collectively, our findings demonstrate that reducing proadipogenic signaling in thymus via CR may promote thymopoiesis during aging.

In 2006, ~500 million people world-wide were 65 years or older. According to current predictions, the aging population will rise dramatically and by the year 2030 approximately one in eight people will be over the age of 65 (1). Aging of the immune system is critically linked to health and survival as reflected by increased incidence of severe infections, reactivation of chronic infections, waning vaccination responses, and increased incidence of cancers in elderly (2,3). Reduced ability of thymus to produce naive T cells during aging is among the key determinants of reduced immune surveillance in the elderly (4).

[1]This work was supported in part by the Coypu and Pennington Foundation grants to V.D.D. The present work utilized the facilities of the Genomics and Cell Biology and Bioimaging Core facilities supported by National Institutes of Health (NIH) Grant P20 RR-021945 and Cell Biology and Bioimaging Core Facility of the Pennington Biomedical Research Center's Center of Biomedical Research Excellence and Clinical Nutrition Research Unit (NIH P30 DK072476).

2 Address correspondence and reprint requests to Dr. Vishwa Deep Dixit, Laboratory of Neuroendocrine-Immunology, Pennington Biomedical Research Center, 6400 Perkins Road, Baton Rouge, LA 70808. Vishwa.Dixit@pbrc.edu.

Disclosures
The authors have no financial conflicts of interest.

Compared with human memory T cells that undergo homeostatic expansion during aging, the naive T cells produced from thymus express 10 times (10^7) the number of different TCR β-chains, each paired with 100 different α-chains (5). Hence, the loss of naive T cells from thymus in the elderly results in constriction of TCR repertoire diversity, and a consequent inability to recognize new strains of infections or self Ags generated as a result of malignancy (6,7). During physiological aging, the total peripheral T cell pool is maintained by homeostatic expansion of preexisting T cells due to deficits in replenishment by thymic export (8,9). Consequently, T cell repertoire is reduced with an expansion of memory phenotype T cells and thereby limits a host's ability to mount responses against new antigenic challenges like influenza virus (10). Therefore, the ability to increase naive T cell production from the aged is critical to all aspects of immunity, including affecting the Ab production and cell-mediated immunity (11,12). Interestingly, despite massive replacement of thymus with adipose tissue, the aging thymus still retains limited capacity for generating naive T cells (13,14), suggesting that restoration of thymic function may be achievable.

The immune and metabolic systems are tightly coupled to each other via common receptor and ligand expression (15,16,17,18). Signals emanating from the immune system affect the metabolic axis and, reciprocally, changes in the energy balance exert potent immunomodulatory actions (19). We have demonstrated that orexigenic peptide ghrelin, a sensor of negative energy balance, reduces inflammation (20) and enhances thymopoiesis during aging (21). The aged mice infused with ghrelin exhibited a reduction in lipid-expressing cells in the thymus, while ghrelin-deficient animals developed excess thymic adiposity (22). These studies provided initial evidence that deficient ghrelin-signaling induces expression of proadipogenic genes in thymus, providing further support to the hypothesis that the presence of intrathymic adipocytes is inversely linked with thymopoiesis (22). However, the mechanisms of ectopic adipocyte development in thymus remains poorly understood.

Induction of negative energy balance via caloric restriction remains one of most robust nongenetic means of extending health span across several species (23,24). Several studies have shown that calorie restriction (CR)[3] potentiates thymic function (25). However, the mechanism of CR's prothymic effects remains to be elucidated. Based on our previous findings that the CR-induced hormone ghrelin (26) can regulate thymic adiposity (22), we hypothesized that CR specifically inhibits the proadipogenic transcriptional machinery in the aging thymus.

Given that thymic adiposity is a key feature of age-related thymic involution (27,28), we examined whether the prolongevity metabolic intervention CR retards the mechanisms governing the generation of thymic adipocytes. Here, we provide novel evidence that CR specifically inhibits the age-related adipogenic programming of thymic stroma and preserves thymopoiesis.

Materials and Methods

Mice and calorie restriction

Female CR (n = 24) mice and ad libitum (AL) fed (n = 24) 12- to 26-mo-old C57B6L/J mice were purchased from the National Institute on Aging aging rodent colony. The CR was initiated at 14 wk of age at 10% restriction, increased to 25% restriction at 15 wk, and to 40% restriction at 16 wk, where it was maintained throughout the life of the animal. Mice were maintained on

[3]Abbreviations used in this paper: CR, calorie restriction; AL, ad libitum; DL1, Delta-like-1; EMT, epithelial-mesenchymal transition; ETP, earliest thymocyte progenitor; EVA, early V antigen; FABP4/aP2, fatty acid-binding protein-4; FSP-1, fibroblast-specific protein-1; MDI, 3-isobutyl-1-methylxanthine and dexamethasone with insulin; PDGF, platelet-derived growth factor; PPARγ, peroxisome proliferator-activated receptor γ; TEC, thymic epithelial cell; TREC, TCR excision circle; TSC, thymic stromal cell; XOR, xanthine oxidoreductase.

the CR diet during transit and sacrificed after 1 wk of rest. We also utilized 3- to 4-mo-old female C57B6L/J mice as a control. The mice were maintained under specific pathogen-free conditions of Pennington Biomedical Research Center's animal facility using protocols approved by the Institutional Animal Care and Use Committee.

Isolation of organs and cell suspension

After sacrifice, thymi and spleen were isolated, weighed, and fixed with 20% sucrose solution for cyrosection or frozen for RNA extraction. The spleens and thymi were dispersed on nylon mesh for single-cell preparation. The dispersed cells were treated with ACK solution and prepared as single-cell suspensions for flow cytometry analysis. Some femurs were fixed in Bouin's solution for making paraffin sections.

Abs and immunoconjugates

For FACS analysis the following Abs (from eBioscience) were used: CD4-PerCP, CD8-allophycocyanin, CD44-FITC, CD44-allophycocyanin, CD4-PE, anti-CD11b-PE, Gr-1 PE, CD45R-PE, CD3-PE, CD8-PE, CD8-allophycocyanin, $\alpha\beta$TCR-PE, $\gamma\delta$TCR-PE, pan-NK-PE, NK1.1-PE, CD11c-PE, CD19-PE, Ter119-PE, CD127-PE, CD25-allophycocyanin, CD25-PE, and c-Kit-FITC. PDGFR-α, ERTR7, and peroxisome proliferator-activated receptor γ (PPARγ; E-8) were from Santa Cruz Biotechnology.

Flow cytometry

For the detection of naive T cells in spleen, 2×10^6 splenocytes were incubated with CD4-PerCP, CD8-allophycocyanin, CD44-FITC, and CD4-PE for 30 min on ice. To identify earliest thymocyte progenitors (ETPs), 5×10^6 thymocytes were labeled for lineage-positive cells by utilizing PE-conjugated anti-CD11b, Gr-1, CD45R, CD3, CD8, $\alpha\beta$TCR, $\gamma\delta$TCR, pan-NK, NK1.1, CD11c, CD19, Ter119, and CD127 Abs, but no CD4, followed by staining with CD25-allophycocyanin and c-Kit-FITC. The PE-labeled lineage-negative cells lacking CD25, and expressing c-Kit and CD44, were designated as ETPs as previously described (29,30). All Abs were purchased from eBioscience. The neutral lipids in CD45-negative cells were stained using LipidTOX Green (Invitrogen). All FACS analysis was performed on a FACSCalibur (BD Biosciences) using up to four fluorescent channels, and all the FACS data were analyzed by postcollection compensation using FlowJo (Tree Star) software.

Immunohistochemistry

The thymi obtained from mice were flash frozen and cut into 5-μm-thick cryostat sections, followed by fixing with 4% buffered paraformaldehyde. Tissue sections were stained with various combinations of the following primary Abs to mouse Ags: unconjugated rat mAb to TROMA-1 (Developmental Studies Hybridoma Bank), biotin-conjugated mouse mAb to *Ulex europaeus* agglutinin 1 (UEA-1; Vector Laboratories), and unconjugated rat Ab to ERTR7 (HM1086; Cell Sciences). Sections were incubated with the specific Abs conjugated with: Alexa Fluor 488- or Alexa Fluor 594-conjugated polyclonal chicken anti-mouse IgG; Alexa Fluor 488-conjugated polyclonal donkey anti-rat IgG; and Alexa Fluor 488- or Alexa Fluor 594-conjugated polyclonal chicken anti-rabbit IgG (Invitrogen). Nuclei were visualized with DAPI (4′,6-diamidine-2′phenylindole dihydrochloride; Sigma-Aldrich). Negative controls as obtained by occulting the primary Ab or by using an unrelated IgG displayed no specific labeling. Fluorescence mounting solution (Vector Laboratories) was applied to slides and observed with a Zeiss Axioplan 2 microsocpe. Additionally, for the visualization of lipid droplet and adipocyte populations, frozen thymic sections and cultured cells were fixed with 4% buffered paraformaldehyde and then stained with Oil Red O and LipidTOX Green (Invitrogen) for 20 min. Mayer's H&E staining was performed with frozen thymic sections and bone sections deparaffinized using alcohol series and xylene to examine their structure.

Real-time RT-PCR

Total RNA was prepared with RNAzol (Isotex Diagnostics). The cDNA synthesis and real-time RT-PCR were performed as described previously (21,22,31). Real-time RT-PCR analyses were done in duplicate on the ABI Prism 7900 sequence detector *Taq*Man system with the SYBR Green PCR kit as instructed by the manufacturer (Applied Biosystems). The list of real-time PCR primers is shown in Table I.

Western blot analysis and xanthine oxidoreductase (XOR) activity

The Western blot analysis was performed as described previously (31). Briefly, the thymi were lysed in RIPA buffer supplemented with protease and phosphatase inhibitor mixture (Sigma-Aldrich), and protein concentrations of cell lysates were determined. The lysates were diluted with sample buffer, separated on 4–20% Tris-HCl/SDS-polyacrylamide gels (Novex), and electrophoretically transferred to nitrocellulose membranes (Invitrogen). The blots were then incubated with rabbit polyclonal Ab anti-mouse PPARγ (E-8; Santa Cruz Biotechnology), rabbit polyclonal anti-mouse aP2 (2120S; Cell Signaling Technology), and actin-specific mouse mAb (Sigma-Aldrich). Immune complexes were visualized by incubation with specific secondary Abs conjugated to Alexa Fluor 680 (Invitrogen) and membranes were imaged for fluorescence on Odyssey infrared imaging system (LI-COR Biosciences). The XOR activity in thymus was analyzed according to the manufacturer's instruction (Cayman Chemical).

Thymic stromal cell culture

Thymic lobes were minced into small fragments and treated for 1 h at 37°C with an enzymatic mixture containing 1 mg/ml collagenase (Sigma-Aldrich), 0.2 mg/ml DNase type I (Sigma-Aldrich), and 1 mg/ml trypsin EDTA (Invitrogen) in PBS as described previously (32). Cells were spun at 13,000 rpm for 5 min. The pellet was resuspended and 10^6 cells/well were seeded in 6-well or 24-well culture plates and cultured in DMEM nutrient F12 (DMEM/F12 with 15 mM HEPES, $NaHCO_3$, and L-glutamine; Invitrogen) supplemented with 3 μg/ml insulin, 20 ng/ml epidermal growth factor, 100 U/ml penicillin-streptomycin, and 20% FBS. Cultures were maintained at 37°C and 5% CO_2, and the medium was changed twice a week. On 14 day, cells were induced to differentiate by changing the medium to DMEM/F12 containing MDI (10% FBS, 0.5 mM 3-isobutylmethylxanthine, 1 μM dexamethasone, and 1.7 μM insulin), PPAR antagonist (GW9662), and rosiglitazone (Tocris Bioscience; gift by Dr. E. Floyd). After 48 h, the cells were stained with Oil Red O and collected to extract total RNA.

The OP9-DL1 cells were provided by J. C. Zuniga-Pflucker and cultured as described previously (33). The OP9-DL1 cells were treated with proadipogenic cocktail containing MDI, GW9662, or rosiglitazone for 5 days and then with medium containing 1.7 μM insulin alone for 2 days. Thereafter, the MDI was removed and cells were cultured in regular OP9-DL1 conditions in the presence of bone marrow-enriched LSK cells for an additional 2 wk. The T cells were harvested for FACS analysis and OP-DL1 cells were used for preparation of total RNA.

Quantification of signal joint TCR excision circles

The $CD4^+$ T cells were isolated from splenocytes using a mouse $CD4^+$ T cell positive selection kit (Invitrogen). The sorted cells were lysed in 100 mg/L proteinase K (Sigma-Aldrich) for 1 h at 56°C followed by 10 min at 95°C. The amount of TCR excision circles (TRECs) was determined by real-time quantitative PCR using the ABI Prism 7900 sequence detector *Taq*Man system (Applied Biosystems). The PCR was performed with mδRec- and ψJα-specific primers and mδRec-ψJα fluorescent probe as described previously (14,21). The standard curves for murine TRECs were generated by using δRec ψJα TREC PCR product cloned into a pCR-XL-TOPO plasmid, a gift from Dr. Gregory D. Sempowski (Duke University Medical Center).

Vβ TCR spectratyping analysis

The analysis of hypervariable CDR3 of *β*-chain offers a practical approach for the global analysis of diversity of TCR repertoire (34). For TCR spectratyping and CDR3 length analysis PCR, a FAM-labeled nested constant *β*-region primer was used in combination with 24 multiplexed forward murine V*β*-specific primers. PCR was performed for 35 cycles with denaturation at 94°C for 30 s, annealing for 55°C for 30 s, and 1 min extension at 72°C. and the PCR products are analyzed on an ABI 3130 genetic analyzer (Applied Biosystems). Each V*β*-J*β* rearrangement is visualized by six to eight peaks, and each peak represents one or a set of T cell clones bearing the same CDR3 length. Each peak was analyzed and quantified with ABI Prism GeneScan analysis software (Applied Biosystems), based on size and density. Data were used to calculate the area under the curve for each V*β* family. Each peak, representing a distinct CDR3 of a certain length, was quantified with statistical software (BioMed Immunotech).

Proliferation and MTT assay

The splenic $CD4^+$ cells from 26-mo-old animals were isolated using T cell selection column (R&D Systems). The 2×10^5 cells/well were cultured in flat-bottom 96-well plates coated with anti-CD3 and anti-CD28 Abs (BD Pharmingen) in RPMI 1640 media supplemented with 10% FCS and 0.1% antibiotic/antimycotic mixture. Forty-eight hours after culture, cells were harvested for preparation of RNA. The rest of the wells were used for MTT assay to measure proliferation via mitochondrial dehydogenase activity according to the manufacturer's instructions (CGD1; Sigma-Aldrich).

Statistical analyses

The results are expressed as the mean ± SEM. The differences between means and the effects of treatments were determined by one-way ANOVA using Tukey's test (SigmaStat), which protects the significance ($p < 0.05$) of all pair combinations.

Results

Age-related increase in intrathymic adipocyte development is blocked by CR

We utilized 2- to 12- and 18-mo-old AL and CR fed C57B6L/J female mice to investigate the initiation of age-related adipogenic programming in the thymus. Compared with 2-mo-old animals, the thymus of 12-mo-old mice displayed an increase in large lipid vacuole-containing mature adipocytes along with smaller lipid-bearing cells in the medulla as well as cortex (Fig. 1*A*). Interestingly, the loss of adipocytes by CR was associated with markedly dense cellularity in cortex as well as medulla (Fig. 1*A*). During aging, ectopic adipocytes also develop within the bone marrow. However, unlike thymus, CR did not block the adipocyte development in aging bone marrow, but instead caused a marked reduction in adipocyte size in femur (Fig. 1*B*).

Aging over the first year of life in mice was associated with an increase in the total body adiposity, while the 12-mo-old CR mice had body weights similar to those of young mice (Fig. 1*C*). We observed that organ sizes (liver, spleen) in CR mice were reduced (data not shown) in proportion to their body size. Therefore, when corrected for body weight, the CR thymi had a higher somatic index (Fig. 1*C*). Also, the total thymic cellularity from CR mice was not significantly greater in 12-mo-old AL mice (Fig. 1*C*); instead, the smaller thymic space was densely packed with thymocytes (Fig. 1*A*). Additionally, we did not observe any alterations in double-negative, single-positive, or double-positive frequencies (data not shown).

We next determined whether maintenance of thymic architecture by CR prevents the age-related reduction in naive T cells. Consistent with established findings (8,9,35), analysis of

naive and effector/memory T cells in the spleen revealed a marked reduction in naive CD4 and CD8 cells and expansion of effector/memory population with age. Interestingly, similar to chronic CR in primates (36), CR in mice also led to a marked preservation of both CD4 and CD8 naive T cells and prevented the age-related expansion of effector/memory populations (Fig. 1*D*).

CR prevents the age-related alteration in the thymic stromal microenvironment

Age-related thymic involution is known to lead to loss of thymic epithelial cell (TECs) and increase in fibroblasts (37–40). Compared with young mice, in 12-mo-old animals we found a reduction in cortical TECs as well as loss of organization of medullary TECs. CR prevented the age-related loss of cortical TEC and medullary TEC organization (Fig. 2*A*). The mRNA levels of early V Ag (EVA), a constitutively cortical TEC expressed gene, have been used as a surrogate marker to quantify epithelial cell regeneration in aging thymus (41). Consistent with an increase in keratin 8^+ cortical TECs, we observed that CR significantly increases the EVA expression in the older thymi without affecting the Aire expression, a medullary TEC subset-specific gene (Fig. 2*B*).

Thymopoiesis is dependent on homing of bone marrow-derived lymphoid progenitor cell populations (42) into thymus. The TEC-derived chemokines CXCL12 and CCL25 are critical for recruitment and homing of lymphoid progenitors in thymus (43–46). We observed that the aging thymus displayed a marked reduction in CXCL12 mRNA expression, which was restored by CR (Fig. 2*B*). Additionally, CR increased the CCL25 expression in aging thymus (Fig. 2*B*). Further analysis of thymic cryosections of 18-mo-old mice revealed a higher immunostaining for lipid-bearing $ERTR7^+$ thymic fibroblasts (Fig. 2*C*). Interestingly, the ERTR7 and intrathymic lipid accumulations in 18-mo-old mice were markedly reduced when these mice were maintained on CR (Fig. 2*C*). Consistent with immunohistological data, the FACS analysis of thymic digests revealed that CR significantly decreased the $CD45^-lipid^+$ cells in age-matched 18-mo-old mice (Fig. 2*D*).

Using genetic fate-mapping approaches, we have recently demonstrated that TECs can transition to fibroblasts via the process of epithelial-mesenchymal transition (EMT) (22). We therefore hypothesized that CR-induced increases in TECs and reductions in fibroblasts may be mediated through the inhibition of EMT. Interestingly, we found that thymic aging was associated with increase in the pro-EMT regulators fibroblast-specific protein-1 (FSP-1)/S100A4, FoxC2, vimentin, and N-cadherin (Fig. 2*E*). Consistent with our hypothesis, CR blocked the age-related increase in pro-EMT genes (Fig. 2*E*). Taken together, these data suggest that CR may also inhibit the generation of local fibroblasts in aging thymus and prevents the age-related deterioration of thymic stromal cell microenvironment.

CR specifically inhibits the age-related increase in intrathymic proadipogenic transcriptional machinery

The transcription factor PPARγ is necessary and sufficient for commitment of fibroblast and preadipocytes to adipocytes (47–49). Given our findings that CR prevents the development of lipid-bearing fibroblasts in aging thymus, we next asked whether PPARγ is involved in age-related thymic adiposity. We found that PPARγ protein was markedly increased by 12 mo of age in thymus (Fig. 3*A*). Interestingly, CR blocked the age-related elevation of γ1 and γ2 splice variant isoforms of PPAR (Fig. 3*A*) in thymus. Additionally, CR also significantly inhibited a key adipogenic lipid chaperone, adipocyte fatty acid binding protein aP2 or FABP4 (47), in thymus (Fig. 3*A*). Furthermore, the age-related increase in thymic PPARγ and aP2 mRNA expression was also reduced by CR (Fig. 3*B*).

Considering that fibroblasts can be readily induced to develop into adipocytes, we next investigated whether CR prevents the expression of PPARγ protein in PDGFRα^+ thymic fibroblasts. Consistent with our hypothesis, we found that compared with age-matched 12-mo-old AL fed mice, CR reduced the frequency of PDGFRα^+PPARγ^-, PDGFRα^+PPARγ^+, as well as PDGFRα^-PPARγ^+ cells in thymus (Fig. 3*C*). We also investigated whether CR blocks proadipogenic regulators globally. We observed that CR did not inhibit PPARγ mRNA expression in white adipose tissue or brown adipose tissue of 12-mo-old mice (data not shown), suggesting that the effects of CR on inhibition of thymic PPARγ are organ specific.

Given that CR-induced inhibition of thymic PPARγ is associated with reduction of lipid-bearing fibroblasts and adipocytes, we tested the causality of this relationship using an in vitro primary thymic stromal cell (TSC) culture model. Surprisingly, we observed that upon culture, ~92% of CD45$^-$ TSCs exhibited fibroblast-like phenotype and were ERTR7$^+$ (Fig. 4, *A* and *B*). The mechanism of loss of TEC and emergence of fibroblast in culture are currently under investigation in our laboratory. However, this culture system provided us an in vitro cellular model to study mechanism of adipogenesis of primary thymic fibroblasts. The treatment of these ERTR7$^+$ thymic fibroblasts with PPARγ ligand rosiglitazone led to accumulation of large lipid droplets, reminiscent of an adipocyte phenotype (stained by LipidTOX Green) (Fig. 4*B*). Compared with vehicle (DMSO)-treated control cells, the incubation of thymic fibroblasts with adipogenic cocktail (MDI) containing dexamethasone (1 μM), 3-isobutyl-1-methylxanthine (MIX, 0.5 mM), and insulin (1.67 μM) also induced robust adipogenesis (Fig. 4*C*). The Oil Red O staining of neutral lipids revealed differentiation of thymic fibroblasts into adipocytes upon MDI treatment, which was blocked in the presence of the specific PPARγ antagonist GW9662 (Fig. 4*C*). These data show that PPARγ directly regulates the adipocyte development of thymic fibroblasts and suggest that CR-induced reduction in thymic PPARγ may prevent the development of age-related thymic adiposity.

The PPARγ-driven adipogenesis of thymic fibroblasts is dependent on XOR

XOR generates reactive oxygen species and has recently been identified as a novel upstream regulator of PPARγ (50). This prompted us to test whether the age-related increase in thymic XOR activity regulates PPARγ and adipogenesis of thymic stromal elements. Interestingly, similar to our findings with PPARγ, the XOR mRNA was significantly increased in aging thymus, while CR restored this age-related elevation to the levels found in young mice (Fig. 5*A*). In addition to its mRNA expression, age-related increase in XOR activity in thymus was also blocked by CR (Fig. 5*B*). Furthermore, the XOR mRNA expression was significantly increased in the TSCs induced to undergo adipogenesis, while specific PPARγ antagonist restored the XOR expression to control nonadipogenic cells (Fig. 5*C*).

We next tested whether the XOR inhibition can prevent PPARγ ligand-dependent transition of TSCs into adipocytes. Treatment of thymic fibroblasts with XOR inhibitor diphenyleneiodonium prevented the PPARγ ligand (rosiglitazone)-dependent adipocyte development (Fig. 5*D*). Consistent with the observation that XOR regulates PPARγ-dependent transition of stromal cells into adipocytes, the XOR inhibitor blocked the expression of proadipogenic transcripts PPARγ, perilipin, PPARγ angiopoietin related (PGAR), and CD36 (Fig. 5*E*). Collectively, these data suggest that XOR may be one of the key regulators of PPARγ expression in aging thymus and during CR.

PPARγ-dependent adipogenesis of stromal cells compromises T cell development

In an effort to test the consequence or impact of elevated PPARγ signaling on T cell development capacity of stromal cells, we used the OP9-DL1 cell model. The stromal-epithelial cellular phenotype is critical for T cell development (51). However, removal of TSCs from three-dimensional thymic meshwork results in loss of Notch ligand Delta-like-1, (DL1) and

hence in ex vivo conditions, the TSCs are unable to support the development of T cells from lymphoid progenitors (51). The enriched $Lin^{-}Sca I^{+}c\text{-}Kit^{+}$ (LSK) cells when cocultured with OP9-DL1 cells differentiate to $CD4^{+}CD8^{+}$ (double-positive) and single-positive T cells (33). We demonstrate that OP9-DL1 cells can transition into adipocytes in the presence of rosiglitazone or MDI (Fig. 6*A*). We next induced the OP9-DL1 cells to differentiate into adipocytes in the presence of specific PPAR*γ* ligand rosiglitazone, MDI, and MDI together with PPAR*γ*-specific antagonist GW9662 for 1 wk. After 1 wk of culture and stromal cell differentiation into adipocytes, the adipogenic media were replaced, and OP9-DL1 cells were cocultured in presence of enriched bone marrow-derived LSK cells, IL-7, and Flt3 ligand. Interestingly, we observed that both rosiglitazone- and MDI-induced OP9-DL1 adipocytes were severely compromised in their ability to support the development of lymphoid progenitors to DP cells (Fig. 6*B*). In presence of PPAR*γ* antagonist GW9662, the MDI-induced reduction in double-positive cell numbers was restored to control levels, suggesting a PPAR*γ*-specific mechanism for inhibition of T cell development (Fig. 6*B*).

To further confirm the specificity of PPAR*γ* pathway in adipogenic OP9-DL1 cells, we next studied the expression of lipoprotein lipase and phosphoenolpyruvate carboxykinase, the downstream target genes indicative of PPAR*γ* activity (52,53). We observed that rosiglitazone as well as MDI led to significant increases in PPAR*γ* target genes in adipogenic OP9-DL1 cells via PPAR*γ*-specific pathway (Fig. 6, *C* and *D*). Furthermore, the real-time PCR analysis of OP9-DL1 cells revealed that stromal adipogenesis reduced the expression of Jag1, Jag2, stem cell factor and keratinocyte growth factor without affecting thymic stromal-derived lymphopoietin (TSLP) expression and DL-1 expression (data not shown) in a PPAR*γ*-dependent fashion (Fig. 6, *E* and *F*). Thus, our data suggest that loss of stromal cell signatures via a PPAR*γ* pathway may compromise their ability to support T cell development.

Inhibition of proadipogenic regulators by CR is associated with reduced immunosenescence

We have recently demonstrated that deficient ghrelin signaling accelerates thymic involution (21) with elevated expression of proadipogenic regulators, including PPAR*γ* (22). Since CR reduced the age-related adipogenic programming of TSCs, we next studied the consequence of improved thymic microenvironment on thymopoiesis. It has been demonstrated that ETPs, $Lin^{-}CD44^{+}c\text{-}Kit^{high}$ cells, give rise to T cells upon entry at the cortico-medullary junction in the thymus and their numbers decline with age (29,30). Consistent with our results that CR maintains TECs and critical chemokines required for progenitor homing, we found a significant increase in the ETP cells (Fig. 7*A*). The reduction of bone marrow adipocyte cell size by CR was not associated with any change in bone marrow $Lin^{-}Sca I^{+}c\text{-}Kit^{+}$ (LSK) cells (data not shown). Furthermore, the quantitative real-time PCR of splenic $CD4^{+}$ cells revealed that CR significantly increased the TREC numbers in 12-mo-old animals (Fig. 7*B*), suggesting increased thymopoiesis. We next tested whether the CR-induced naive T cell production is reflected in improved T cell function. Compared with 26-mo-old AL fed mice, the $CD4^{+}$ T cells derived from age-matched CR animals displayed significant increase in proliferation (Fig. 7*C*) and IL-2 expression (Fig. 7*D*) in response to TCR ligation.

The reduction in naive T cell output and expansion of memory T cells with aging causes reduced TCR diversity, leading to functional deficits in adaptive immune responses (8,9,11,12). To further investigate the functional consequences of thymic renewal postreduced adipogenesis, we studied TCR diversity of peripheral $CD4^{+}$ T cells by measuring the distribution of lengths of the CDR3. Although a lower resolution approach, the TCR spectratyping allows the global analysis of TCRs of the sampled T cell population (34). A polyclonal diverse TCR V*β* family is characterized by Gaussian distribution of peaks, while a skewed profile is distinguished by deviations from Gaussian distribution (6) and aberrant amplification of peaks (Fig. 7*E*). The Gaussian distribution profiles were translated into probability distributions as functions of the

area under the curve for each CDR3 length as described previously (54). By these methods we demonstrate quantitatively that the reduction in thymoadipogenesis by CR led to a significant improvement in TCR diversity profile during aging (Fig. 7*F*).

Discussion

Calorie restriction is a potent metabolic intervention that induces a state of chronic negative energy balance and robustly extends mean and maximal lifespan in experimental animals (23,24). There is a large body of data from animal models that suggest that CR has a significant impact on various arms of the immune system. Most of the reports suggest that CR improves many parameters of immune responses (19,25,40), such as responses of T cells to mitogens, NK cell activity, CTL activity, and the ability of mononuclear cells to produce proinflammatory cytokines (55,56). Additionally, long-term CR in primates enhances thymopoiesis and improves the TCR diversity (36). However, the mechanism of the effects of CR on age-related thymic involution process is incompletely understood. Here we present evidence that CR preserves the thymic microenvironment and prevents the age-related increase in PPARγ-dependent adipogenic progression of thymic stroma. Inhibition of PPARγ and its upstream activator XOR by CR is associated with increased thymopoiesis. The thymic fibroblasts undergo XOR- and PPARγ-dependent differentiation into adipocytes in vitro. Using a OP9-DL1 stromal cell model, we present direct evidence that liganded PPARγ compromises the T cell development that can be restored by blocking PPARγ. Furthermore, inhibition of thymic adipogenesis by CR was associated with increased ETP frequency, enhanced thymic output, and prevention of age-related restriction of the peripheral TCR repertoire diversity.

Dramatic age-related changes occur in thymic microenvironment. The $CD45^-$ stromal cell number in 12-mo-old animals decreases along with a reduction in MHC class II expression on epithelial cell adhesion molecule-expressing TECs (37,38). Recent evidence suggests that apart from TECs, the stromal fraction of thymic cellularity is also comprised of fibroblasts, and loss of TECs with age is associated with a concomitant increase in fibroblasts (37,39,40). Chemical-shift magnetic resonance imaging analyses of middle-aged human thymus revealed almost complete replacement of thymic space with adipocytes (40). Thymocytes have been demonstrated to control the development of thymic stroma in a stepwise fashion, and the importance of lympho-stromal interactions during thymic development is well recognized (57). Given that the loss of thymocytes precedes development of adipocytes in thymus (14, 22), it is plausible that thymic adipocytes arise secondarily to occupy thymic niches vacated by loss of thymocytes. In RAG^{null} mice, thymus is hypocellular and T cell development is blocked at the $CD44^-CD25^+$ stage with disorganized medulla and abnormal thymic epithelial cells (57,58). Given that thymi from young RAG^{null} mice have equivalent thymocyte numbers as do 28-mo-old C57B6L/J mice (3 to 5×10^6), we expected to observe a large number of thymic adipocytes in RAG^{null} animals. However, histological analysis of 4-wk-old RAG^{null} mice revealed no spontaneous increase in intrathymic adipocytes (data not shown). Additionally, the SCID/IL-2R γ-chain-null mice also have severe thymic hypocellularity (59, 60); however, similar to RAG^{null} mice, no adipocytes have been reported within the thymic space (59,60). These data suggest that the healthy aging process initiates a specific set of events to promote intrathymic adipocyte development.

We have recently demonstrated that ablation of ghrelin signaling led to loss of TECs and an increase in adipogenic fibroblasts in thymus. Using *FoxN1:Cre*$^{+/-stop/floxROSA[Lacz]}$ double-transgenic mice, where the FoxN1-expressing TECs are indelibly marked with LacZ, we reported that TECs can transition into adipocytes via the process of EMT (22). Interestingly, we also found that a population of transitional EMT-derived fibroblast cells express PPARγ, suggesting that they may constitute a subset of intrathymic adipogenic precursors (22). Here, we show that CR preserves thymic stroma and inhibits the age-related increase in EMT and

reduces the generation of local thymic fibroblasts. Thus, CR may prevent the age-related transition of TECs to fibroblasts and their further differentiation into adipocytes by reducing proadipogenic regulators (Fig. 8). Fibroblasts are highly plastic, as evidenced by their capacity to be induced to a pluripotent stem cell state by introduction of oct4, sox2, c-myc, and klf4 (61). Together with our recent report that a subset of TECs transition to fibroblasts via the EMT process (22), our current data suggest that PPARγ-driven adipogenic mechanism in thymic fibroblasts may contribute to age-related thymic involution.

It is well known that nuclear receptor PPARγ is required for insulin sensitivity and is necessary and sufficient for adipogenesis (48). PPARγ is regarded as a primary transcription factor for white adipose tissue differentiation and is induced during adipocyte development, and nonadipogenic cells with forced PPARγ expression undergo adipogenesis (47–49). Additionally, in response to chronic positive energy balance, fibroblasts differentiate into adipocytes in the white adipose tissue and serve as an energy storage source by accumulating lipids (47). The purpose of adipocytes is to regulate energy homeostasis and store esterified lipids in a manner that is nontoxic to cells and organisms, while the function of thymus is to produce T cells. Thymus is the major immune organ that is largely replaced with fat at an early age independent of adiposity or disease in humans (40). Given that the function of thymus is to establish and maintain T cell arm of immunity and not to regulate energy homeostasis, the adipocyte development within the thymic space is intriguing. Our findings that CR specifically regulates PPARγ-driven thymic adipogenesis without affecting the global PPARγ are consistent with the maintenance of insulin sensitivity in CR mice. Interestingly, unlike thymus, in bone marrow, CR reduced the adipocyte cell size but did not prevent the adipocyte formation. Reduction in adipocyte size is known to result in greater metabolic efficiency and higher insulin sensitivity (62). This raises the possibility that presence of adipocytes in bone marrow may have a function in regulating local energy balance. Furthermore, the effects of CR on proadipogenic genes appear to be quite specific and dependent on function and nature of adipose and lymphoid microenvironment.

Maintenance of thymic stromal cell microenvironment by CR, presumably through inhibition of EMT, may be one potential mechanism that maintains thymic function during aging. Given that secondary mesenchymal or fibroblast-like cells generated via EMT are multipotent (63), it is likely that these or other fibroblast cells in thymus are specifically driven into adipogenic fate because of age-related increase in PPARγ. Age-related progression of such cellular transition mechanisms and adipogenic cascades may culminate in conversion of thymus into “fatty tissue” in elderly. The testing of this hypothesis through aging of defined genetic animal models may provide definitive in vivo information to solve the puzzle of thymic adiposity.

Caloric restriction robustly prevented the age-related decrease in peripheral naive T cells, which was reflected in elevated TREC numbers. Interestingly, CR also blocked the age-related restriction of TCR repertoire. It is well known that the naive $CD4^+$ T cells from aged animals and humans show reduced IL-2 production, proliferation, and helper functions (64–67). We therefore tested the effect of CR on T cell proliferation and IL-2 expression in 26-mo-old mice that display advanced thymic involution. We reasoned that, by 26 mo, mice are expected to develop greater thymic involution, and if the effects of CR on thymopoiesis in 18 mo of age are robust and inhibition of thymic adipogenic mechanisms has long-term consequence for thymic microenvironment, then the 26-mo-old mice on CR should also have reduced T cell senescence. Therefore, the ability of CR to increase T cell proliferation and IL-2, markers of T cell senescence, provides evidence that CR maintains this key function in aged mice. However, despite the marked improvement of thymic function and reduction in immunosenescence, aged mice on CR are unable to withstand influenza infection (68). This study further underscores that a positive energy balance is required for efficient adaptive immune response and robust T cell function under catabolic conditions induced by infection.

The chronic negative energy balance induced by CR may diminish the energy reserves, negating the benefits elicited by the improvement in T cell diversity during aging. Also, the additional in vivo models to evaluate T cell response and cytokine production on chronic CR may provide direct evidence of the role of CR in mitigating age-related immunosenescence. Additionally, it would be important to determine whether shorter periods of CR that do not deplete peripheral energy stores can inhibit or delay age-related thymic function and offer protection from infectious challenges. However, it is important to consider that in several chronic illnesses or hematopoietic stem cell transplantation conditioning regimens, the elderly patients already have anorexia and frailty, and recommending CR to enhance naive T cell production is not advisable. Therefore, identification and development of compounds that mimic the biology of CR could help uncover novel pathways to enhance thymopoiesis.

Taken together, we demonstrate that CR inhibits adipose tissue development in the thymus by regulating the PPARγ pathway. Various attempts have been made to regenerate the aging thymus through the use of approaches targeted specifically toward the growth factors, lymphoid progenitors, thymocyte subsets, and thymic stromal cells. Our present findings provide further support to the hypothesis that inhibition of thymoadipogenesis may represent an additional strategy to prevent or even reverse age-related thymic involution in the elderly.

Acknowledgments

We thank Drs. Avinash Bhandoola, Donald K. Ingram, and Roy Martin for thoughtful discussions. We also thank Anthony Ravussin, Chiaki Nakata, Rachel Ohlmeyer, and Wubing Ye in the Dixit Laboratory for excellent technical assistance.

References

1. Why population aging matters: global perspective. National Institutes of Health; 2007. publication no. 07-6134
2. Weng NP. Aging of the immune system: how much can the adaptive immune system adapt? Immunity 2006;24:495–499. [PubMed: 16713964]
3. Haynes L, Swain SL. Why aging T cells fail: implications for vaccination. Immunity 2006;24:663–666. [PubMed: 16782020]
4. Linton PJ, Dorshkind K. Age-related changes in lymphocyte development and function. Nat. Immunol 2004;5:133–139. [PubMed: 14749784]
5. Naylor K, Li G, Vallejo AN, Lee WW, Koetz K, Bryl E, Witkowski J, Fulbright J, Weyand CM, Goronzy JJ. The influence of age on T cell generation and TCR diversity. J. Immunol 2005;174:7446–7452. [PubMed: 15905594]
6. Nikolich-Zugich J, Slifka MK, Messaoudi I. The many important facets of T-cell repertoire diversity. Nat. Rev. Immunol 2004;4:123–132. [PubMed: 15040585]
7. Goronzy JJ, Weyand CM. T cell development and receptor diversity during aging. Curr. Opin. Immunol 2005;17:468–475. [PubMed: 16098723]
8. Sprent J, Cho JH, Boyman O, Surh CD. T cell homeostasis. Immunol. Cell Biol 2008;86:312–319. [PubMed: 18362947]
9. Swain S, Clise-Dwyer K, Haynes L. Homeostasis and the age-associated defect of CD4 T cells. Semin. Immunol 2005;17:370–307. [PubMed: 15964201]
10. Yager EJ, Ahmed M, Lanzer K, Randall TD, Woodland DL, Blackman MA. Age-associated decline in T cell repertoire diversity leads to holes in the repertoire and impaired immunity to influenza virus. J. Exp. Med 2008;205:711–723. [PubMed: 18332179]
11. Nikolich-Zugich J. Ageing and life-long maintenance of T-cell subsets in the face of latent persistent infections. Nat. Rev. Immunol 2008;8:512–522. [PubMed: 18469829]
12. Dorshkind K, Montecino-Rodriguez E, Signer RA. The ageing immune system: is it ever too old to become young again? Nat. Rev. Immunol 2009;1:57–62. [PubMed: 19104499]

13. Hale JS, Boursalian TE, Turk GL, Fink PJ. Thymic output in aged mice. Proc. Natl. Acad. Sci. USA 2006;103:8447–8452. [PubMed: 16717190]
14. Sempowski GD, Gooding ME, Liao HX, Le PT, Haynes BF. T cell receptor excision circle assessment of thymopoiesis in aging mice. Mol. Immunol 2002;38:841–848. [PubMed: 11922942]
15. Dixit VD, Mielenz M, Taub DD, Parvizi N. Leptin induces growth hormone secretion from peripheral blood mononuclear cells via a protein kinase C and nitric oxide dependent mechanisms. Endocrinology 2003;144:5595–5603. [PubMed: 12970164]
16. Matarese G, Procaccini C, De Rosa V. The intricate interface between immune and metabolic regulation: a role for leptin in the pathogenesis of multiple sclerosis? J. Leukocyte Biol 2008;84:893–899. [PubMed: 18552206]
17. De Rosa V, Procaccini C, Calì G, Pirozzi G, Fontana S, Zappacosta S, La Cava A, Matarese G. A key role of leptin in the control of regulatory T cell proliferation. Immunity 2007;26:241–255. [PubMed: 17307705]
18. Lago F, Dieguez C, Gómez-Reino J, Gualillo O. Adipokines as emerging mediators of immune response and inflammation. Nat. Clin. Pract. Rheumatol 2007;3:716–724. [PubMed: 18037931]
19. Dixit VD. Adipose-immune interactions during obesity and caloric restriction: reciprocal mechanisms regulating immunity and health span. J. Leukocyte Biol 2008;84:882–892. [PubMed: 18579754]
20. Dixit VD, Schaffer EM, Pyle RS, Collins GD, Sakthivel SK, Palaniappan R, Lillard JW Jr. Taub DD. Ghrelin inhibits leptin- and activation-induced proinflammatory cytokine expression by human monocytes and T cells. J. Clin. Invest 2004;114:57–66. [PubMed: 15232612]
21. Dixit VD, Yang H, Sun Y, Weeraratna AT, Youm YH, Smith RG, Taub DD. Ghrelin promotes thymopoiesis during aging. J. Clin. Invest 2007;117:2778–2790. [PubMed: 17823656]
22. Youm YH, Yang H, Sun Y, Smith RG, Manley NR, Vandanmagsar B, Dixit VD. Deficient ghrelin receptor mediated signaling compromises thymic stromal cell microenvironment by accelerating thymic adiposity. J. Biol. Chem 2009;284:7068–7077. [PubMed: 19054770]
23. Barger JL, Walford RL, Weindruch R. The retardation of aging by caloric restriction: its significance in the transgenic era. Exp. Gerontol 2003;38:1343–1351. [PubMed: 14698815]
24. Bishop NA, Guarente L. Genetic links between diet and lifespan: shared mechanisms from yeast to humans. Nat. Rev. Genet 2007;8:835–844. [PubMed: 17909538]
25. Nikolich-Zugich J, Messaoudi I. Mice and flies and monkeys too: caloric restriction rejuvenates the aging immune system of non-human primates. Exp. Gerontol 2005;40:884–893. [PubMed: 16087306]
26. Yang H, Youm YH, Nakata C, Dixit VD. Chronic caloric restriction induces forestomach hypertrophy with enhanced ghrelin levels during aging. Peptides 2007;10:1931–1936. [PubMed: 17875344]
27. Steinmann GG. Changes in human thymus during aging. Curr. Top. Pathol 1986;75:43–88. [PubMed: 3514161]
28. Flores KG, Li J, Sempowski GD, Haynes BF, Hale LP. Analysis of the human thymic perivascular space during aging. J. Clin. Invest 1999;104:1031–1039. [PubMed: 10525041]
29. Min H, Montecino-Rodriguez E, Dorshkind K. Reduction in the developmental potential of intrathymic T cell progenitors with age. J. Immunol 2004;173:245–250. [PubMed: 15210781]
30. Bhandoola A, Sambandam A. From stem cell to T cell: one route or many? Nat. Rev. Immunol 2006;6:117–126. [PubMed: 16491136]
31. Dixit VD, Weeraratna AT, Yang H, Bertak D, Cooper-Jenkins A, Riggins GJ, Eberhart CG, Taub DD. Ghrelin and the growth hormone secretagogue receptor constitute a novel autocrine pathway in astrocytoma motility. J. Biol. Chem 2006;281:16681–16690. [PubMed: 16527811]
32. Gray DH, Fletcher AL, Hammett M, Seach N, Ueno T, Young LF, Barbuto J, Boyd RL, Chidgey AP. Unbiased analysis, enrichment and purification of thymic stromal cells. J. Immunol. Methods 2008;329:56–66. [PubMed: 17988680]
33. Schmitt TM, Zuniga-Pflucker JC. Induction of T cell development from hematopoietic progenitor cells by Delta-like-1 in vitro. Immunity 2002;17:749–756. [PubMed: 12479821]
34. Pannetier C, Cochet M, Darche S, Casrouge A, Zöller M, Kourilsky P. The sizes of the CDR3 hypervariable regions of the murine T-cell receptor β chains vary as a function of the recombined germ-line segments. Proc. Natl. Acad. Sci. USA 1993;90:4319–4323. [PubMed: 8483950]

35. Dutton RW, Bradley LM, Swain SL. T cell memory. Annu. Rev. Immunol 1998;16:201–223. [PubMed: 9597129]

36. Messaoudi I, Warner J, Fischer M, Park B, Hill B, Mattison J, Lane MA, Roth GS, Ingram DK, Picker LJ, et al. Delay of T cell senescence by caloric restriction in aged long-lived nonhuman primates. Proc. Natl. Acad. Sci. USA 2006;103:19448–19453. [PubMed: 17159149]

37. Gray DH, Tull D, Ueno T, Seach N, Classon BJ, Chidgey A, McConville MJ, Boyd RL. A unique thymic fibroblast population revealed by the monoclonal antibody MTS-15. J. Immunol 2007;178:4956–4965. [PubMed: 17404277]

38. Gray DH, Seach N, Ueno T, Milton MK, Liston A, Lew AM, Goodnow CC, Boyd RL. Developmental kinetics, turnover, and stimulatory capacity of thymic epithelial cells. Blood 2006;108:3777–3785. [PubMed: 16896157]

39. Aw D, Silva AB, Maddick M, von Zglinicki T, Palmer DB. Architectural changes in the thymus of aging mice. Aging Cell 2008;7:158–167. [PubMed: 18241323]

40. Yang H, Youm YH, Rim JS, Galban C, Vandanmagsar B, Dixit VD. Axin expression in thymic stromal cells contributes to age-related increase in thymic adiposity and associated with reduced thymopoiesis independently of ghrelin signaling. J. Leukocyte Biol 2009;85:928–938. [PubMed: 19299626]

41. Min D, Panoskaltsis-Mortari A, Kuro-O M, Holländer GA, Blazar BR, Weinberg KI. Sustained thymopoiesis and improvement in functional immunity induced by exogenous KGF administration in murine models of aging. Blood 2007;109:2529–2537. [PubMed: 17138819]

42. Bhandoola A, von Boehmer H, Petrie HT, Zuniga-Pflucker JC. Commitment and developmental potential of extrathymic and intrathymic T cell precursors: plenty to choose from. Immunity 2007;26:678–689. [PubMed: 17582341]

43. Petrie HT, Zuniga-Pflucker JC. Zoned out: functional mapping of stromal signaling microenvironments in the thymus. Annu. Rev. Immunol 2007;25:649–679. [PubMed: 17291187]

44. Plotkin J, Prockop SE, Lepique A, Petrie HT. Critical role for CXCR4 signaling in progenitor localization and T cell differentiation in the postnatal thymus. J. Immunol 2003;171:4521–4527. [PubMed: 14568925]

45. Williams KM, Lucas PJ, Bare CV, Wang J, Chu YW, Tayler E, Kapoor V, Gress RE. CCL25 increases thymopoiesis after androgen withdrawal. Blood 2008;112:3255–3263. [PubMed: 18694999]

46. Jenkinson WE, Rossi SW, Parnell SM, Agace WW, Takahama Y, Jenkinson EJ, Anderson G. Chemokine receptor expression defines heterogeneity in the earliest thymic migrants. Eur. J. Immunol 2007;37:2090–2096. [PubMed: 17578846]

47. Rosen ED, MacDougald OA. Adipocyte differentiation from the inside out. Nat. Rev. Mol. Cell Biol 2006;7:885–896. [PubMed: 17139329]

48. Tontonoz P, Hu E, Spiegelman BM. Stimulation of adipogenesis in fibroblasts by PPARγ2, a lipid-activated transcription factor. Cell 1994;79:1147–1156. [PubMed: 8001151]

49. Evans R, Barish GD, Wang YX. PPARs and the complex journey to obesity. Nat. Med 2004;10:1–7.

50. Cheung KJ, Tzameli I, Pissios P, Rovira I, Gavrilova O, Ohtsubo T, Chen Z, Finkel T, Flier JS, Friedman JM. Xanthine oxidoreductase is a regulator of adipogenesis and PPARγ activity. Cell. Metab 2007;5:115–128. [PubMed: 17276354]

51. Mohtashami M, Zuniga-Pflucker JC. Cutting edge: Three-dimensional architecture of the thymus is required to maintain Delta-like expression necessary for inducing T cell development. J. Immunol 2006;176:730–734. [PubMed: 16393955]

52. Schoonjans K, Peinado-Onsurbe J, Lefebvre AM, Heyman RA, Briggs M, Deeb S, Staels B, Auwerx J. PPARα and PPARγ activators direct a distinct tissue-specific transcriptional response via a PPRE in the lipoprotein lipase gene. EMBO J 1996;15:5336–5348. [PubMed: 8895578]

53. Tontonoz P, Hu E, Devine J, Beale EG, Spiegelman BM. PPARγ2 regulates adipose expression of the phosphoenolpyruvate carboxykinase gene. Mol. Cell. Biol 1995;15:351–357. [PubMed: 7799943]

54. Gorochov G, Neumann AU, Kereveur A, Parizot C, Li T, Katlama C, Karmochkine M, Raguin G, Autran B, Debré P. Perturbation of $CD4^+$ and $CD8^+$ T-cell repertoires during progression to AIDS

and regulation of the $CD4^+$ repertoire during antiviral therapy. Nat. Med 1998;4:215–221. [PubMed: 9461196]

55. Spaulding CC, Walford RL, Effros RB. Calorie restriction inhibits the age-related dysregulation of the cytokines TNF-α and IL-6 in C3B10RF1 mice. Mech. Ageing Dev 1997;93:87–94. [PubMed: 9089573]
56. Spaulding CC, Walford RL, Effros RB. The accumulation of non-replicative, non-functional, senescent T cells with age is avoided in calorically restricted mice by an enhancement of T cell apoptosis. Mech. Ageing Dev 1997;93:25–33. [PubMed: 9089568]
57. van Ewijk W, Holländer G, Terhorst C, Wang B. Stepwise development of thymic microenvironments in vivo is regulated by thymocyte subsets. Development 2000;127:1583–1591. [PubMed: 10725235]
58. Fehling HJ, von Boehmer H. Early *αβ* T cell development in the thymus of normal and genetically altered mice. Curr. Opin. Immunol 1997;9:263–275. [PubMed: 9099797]
59. Sharfe N, Shahar M, Roifman CM. An interleukin-2 receptor *γ* chain mutation with normal thymus morphology. J. Clin. Invest 1997;100:3036–3043. [PubMed: 9399950]
60. Ohbo K, Suda T, Hashiyama M, Mantani A, Ikebe M, Miyakawa K, Moriyama M, Nakamura M, Katsuki M, Takahashi K, Yamamura K, Sugamura K. Modulation of hematopoiesis in mice with a truncated mutant of the interleukin-2 receptor gamma chain. Blood 1996;87:956–967. [PubMed: 8562967]
61. Wernig M, Meissner A, Foreman R, Brambrink T, Ku M, Hochedlinger K, Bernstein BE, Jaenisch R. In vitro reprogramming of fibroblasts into a pluripotent ES-cell-like state. Nature 2007;448:318–324. [PubMed: 17554336]
62. Greenberg AS, Obin MS. Obesity and the role of adipose tissue in inflammation and metabolism. Am. J. Clin. Nutr 2006;83:461–465.
63. Mani SA, Guo W, Liao MJ, Eaton EN, Ayyanan A, Zhou AY, Brooks M, Reinhard F, Zhang CC, Shipitsin M, et al. The epithelial-mesenchymal transition generates cells with properties of stem cells. Cell 2008;16:704–715. [PubMed: 18485877]
64. Swain S, Clise-Dwyer K, Haynes L. Homeostasis and the age-associated defect of CD4 T cells. Semin. Immunol 2005;17:370–377. [PubMed: 15964201]
65. Thoman ML, Weigle WO. Lymphokines and aging: interleukin-2 production and activity in aged animals. J. Immunol 1981;127:2102–2106. [PubMed: 6457862]
66. Nagel JE, Chopra RK, Chrest FJ, McCoy MT, Schneider EL, Holbrook NJ, Adler WH. Decreased proliferation, interleukin 2 synthesis, and interleukin 2 receptor expression are accompanied by decreased mRNA expression in phytohemagglutinin-stimulated cells from elderly donors. J. Clin. Invest 1988;81:1096–1102. [PubMed: 3127423]
67. Adolfsson O, Huber BT, Meydani SN. Vitamin E-enhanced IL-2 production in old mice: naive but not memory T cells show increased cell division cycling and IL-2-producing capacity. J. Immunol 2001;167:3809–3817. [PubMed: 11564798]
68. Ritz BW, Gardner EM. Malnutrition and energy restriction differentially affect viral immunity. J. Nutr 2006;136:1141–1144. [PubMed: 16614394]

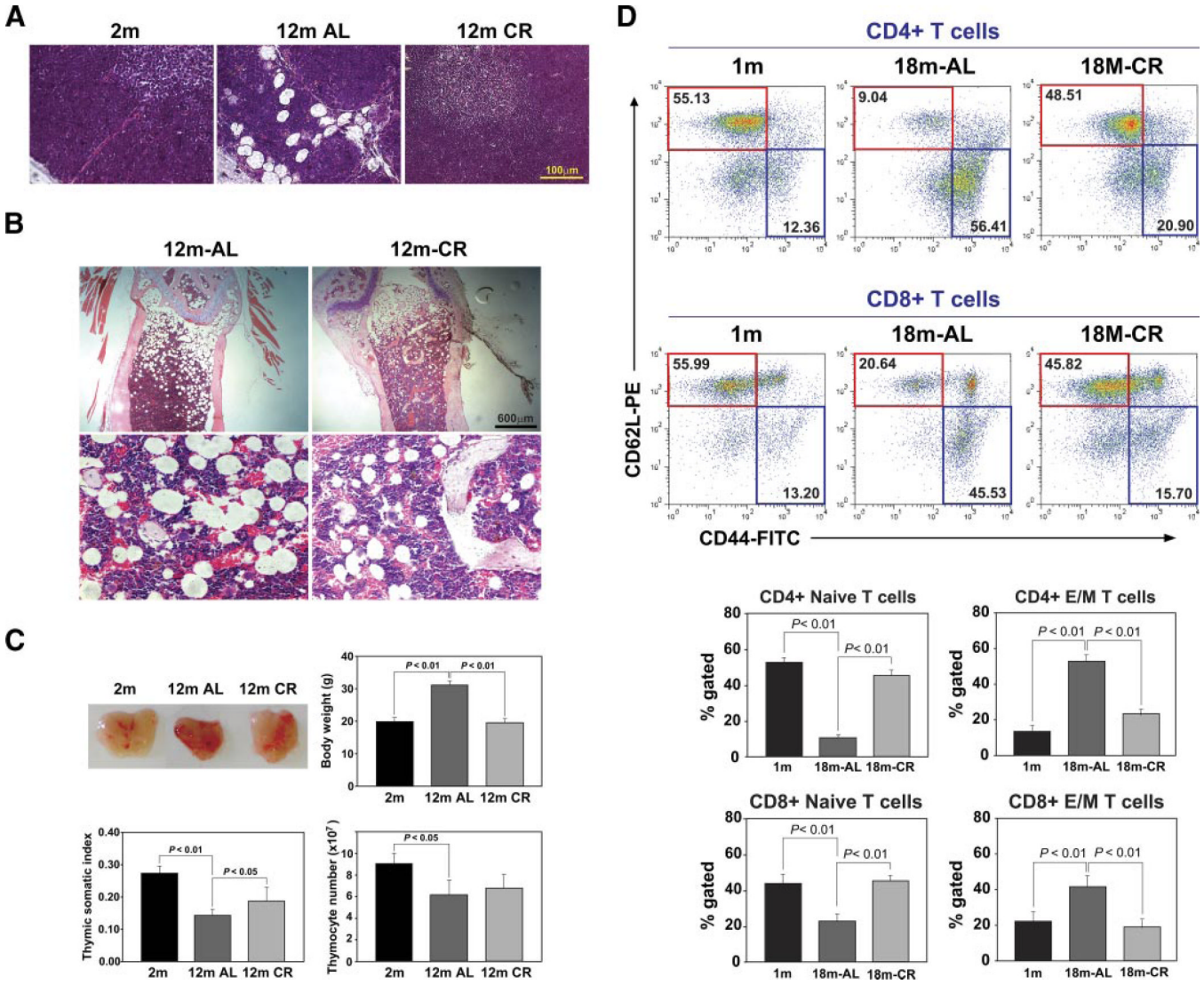

FIGURE 1.

CR reduces thymic adiposity and increases the frequency of naive T cells in aged mice. *A*, H&E staining of representative thymus section ($n = 4$, 12 mo old) shows increase in adipocytes in thymic cortex, medulla, and septum of aging mice. Calorie restriction could block the age-related increase in adipocyte accumulation. *B*, The femurs were decalcified and embedded in paraffin and stained with H&E. *Upper panel*, Images (×100) reveal that CR did not abolish adipocytes in aging bone marrow but led to a marked reduction in cell size. In the AL fed old mice, the bone marrow adipocyte size was ~200 μm (*lower panel*, ×200), which was reduced to almost half by CR. *C*, CR does not increase the thymic size in 12-mo-old mice. The age-related increase in total body weight was prevented by CR. Normalization of body weights with thymic mass (somatic index) displayed a significant increase in thymic somatic index upon CR with no significant difference in total thymocyte counts. The size of thymus of 12-mo-old aging CR mice appeared grossly similar to the young animals. *D*, Analysis of naive and effector/memory (E/M) CD4 and CD8 cells in spleen during aging. The naive ($CD62L^{+}CD44^{-}$) cells (CD4 in *upper panel* and CD8 in *lower panel*) are highlighted in red and effector/memory cells ($CD62L^{-}CD44^{+}$) are in blue boxes. CR significantly increases naive

CD4 and CD8 cells in aging mice. All data are presented as mean (SEM) of six to eight mice per group.

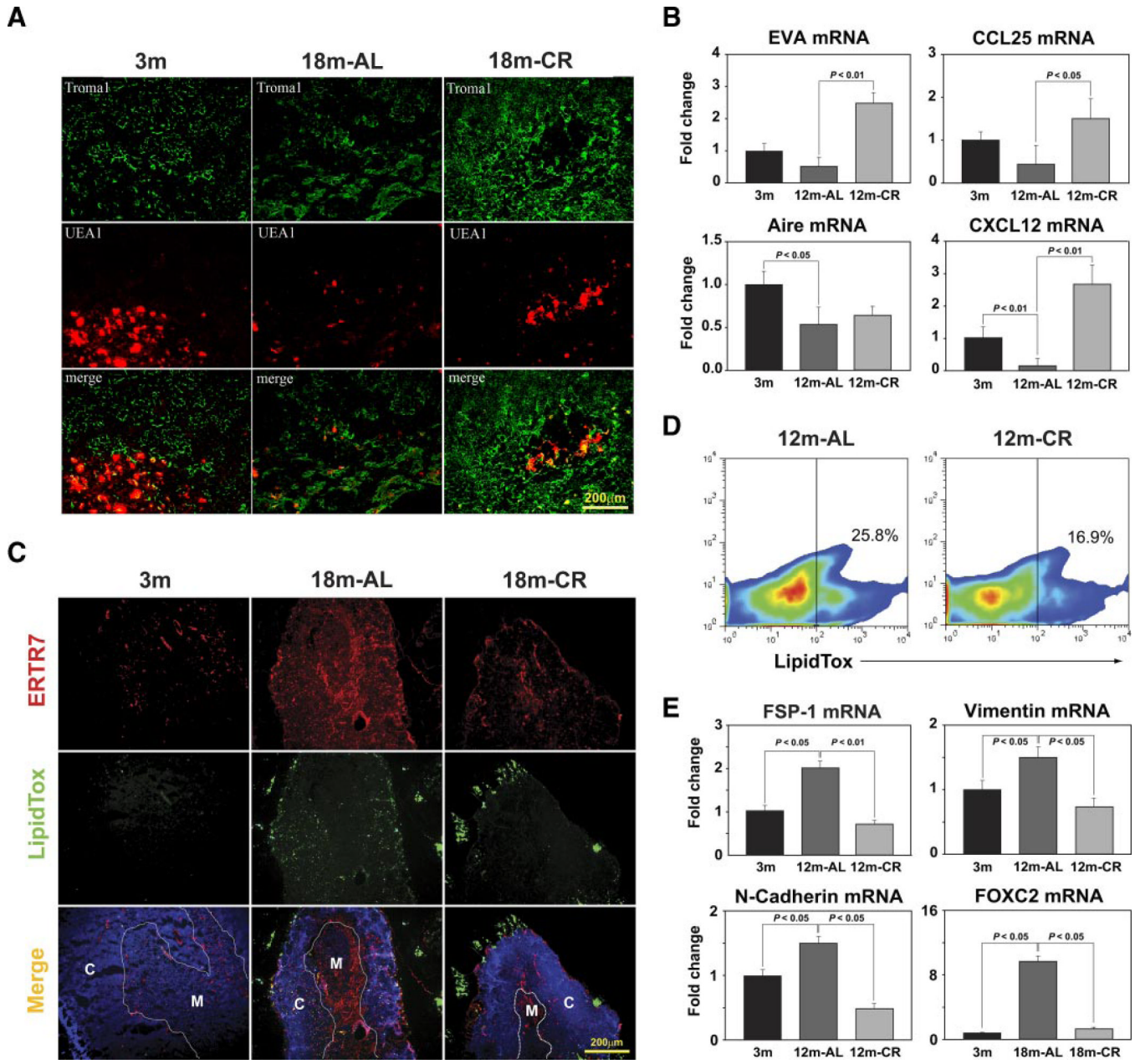

FIGURE 2.

CR maintains thymic stromal microenvironment. *A*, Keratin 8^+ cortical TECs were labeled with anti-TROMA1 Ab and medullary TECs were identified by biotin-conjugated plant lectin *Ulex europaeus* agglutinin 1 (UEA-1). *B*, Real time-PCR analysis of TEC expressed genes. *C*, The thymic cryosections were labeled for fibroblast specific marker ERTR7 (red) and LipidTOX (green). Nuclei were counterstained with DAPI. Representative image from a minimum of four thymi in each group is shown. *D*, The thymi were enzymatically dispersed and labeled with LipidTOX-FITC. The FACS analysis shows that CR decreases the lipid-expressing cells in thymus. A total of three thymi were pooled from each AL and CR group and experiment was repeated twice. *E*, Real time-PCR analysis of pro-EMT regulators FSP-1, vimentin, N-cadherin, and FoxC2 in the thymus. All data are presented as mean (SEM) of six to eight mice per group.

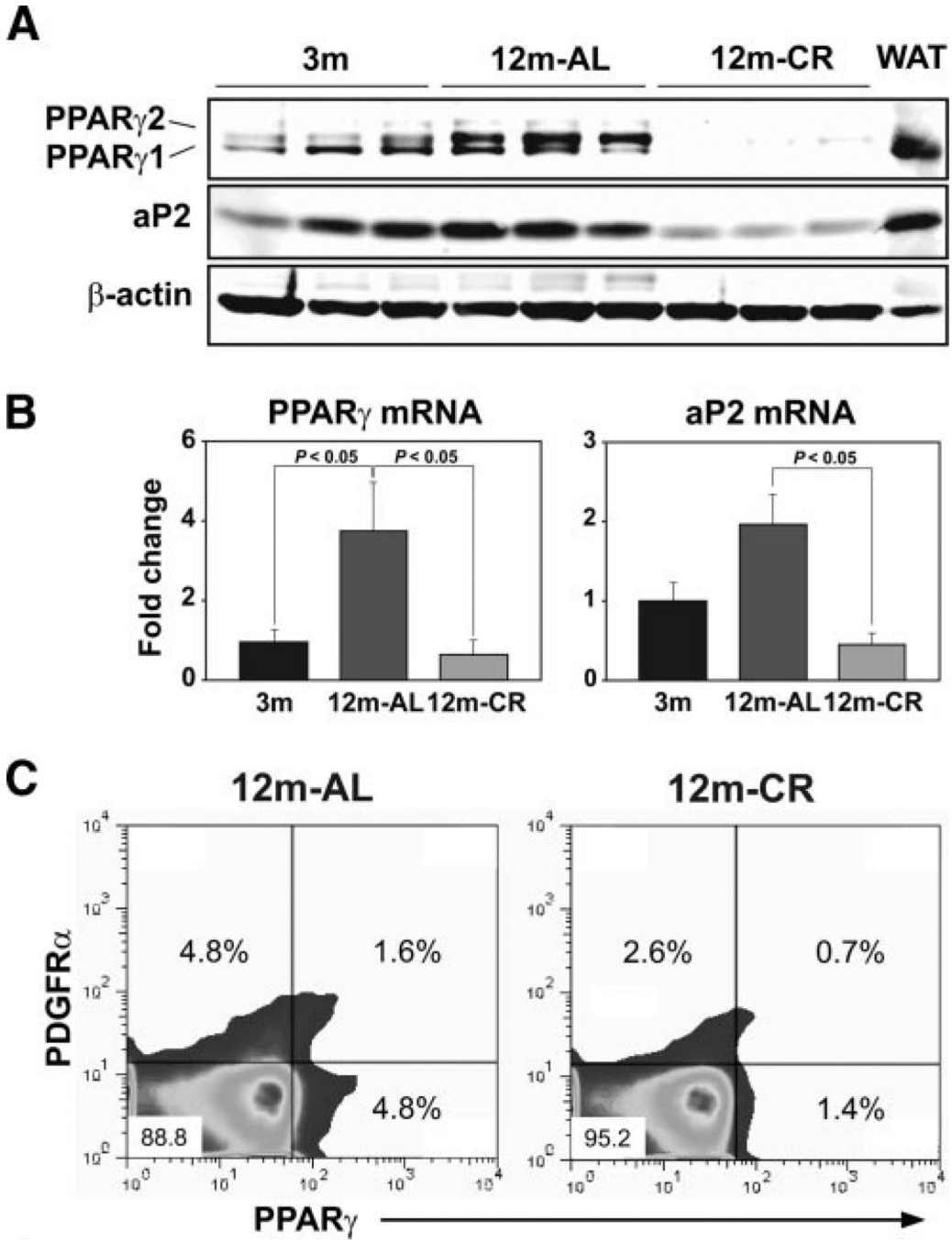

FIGURE 3.

CR inhibits PPAR*γ* in thymus. *A*, Quantitation of PPAR*γ* and aP2 expression by Western blot in thymi and control white adipose tissue (WAT) (*upper panel*). *B*, The mRNA expression was studied by real-time PCR and compared with young (n = 5/group). These data are presented as mean (SEM) of six to eight mice per group. *C*, The thymic digests were gated on CD45-negative cells, and expression of PDGF*α*- and PPAR*γ*-expressing cells is displayed. A total of three thymi were pooled from each AL and CR group and experiments were repeated twice.

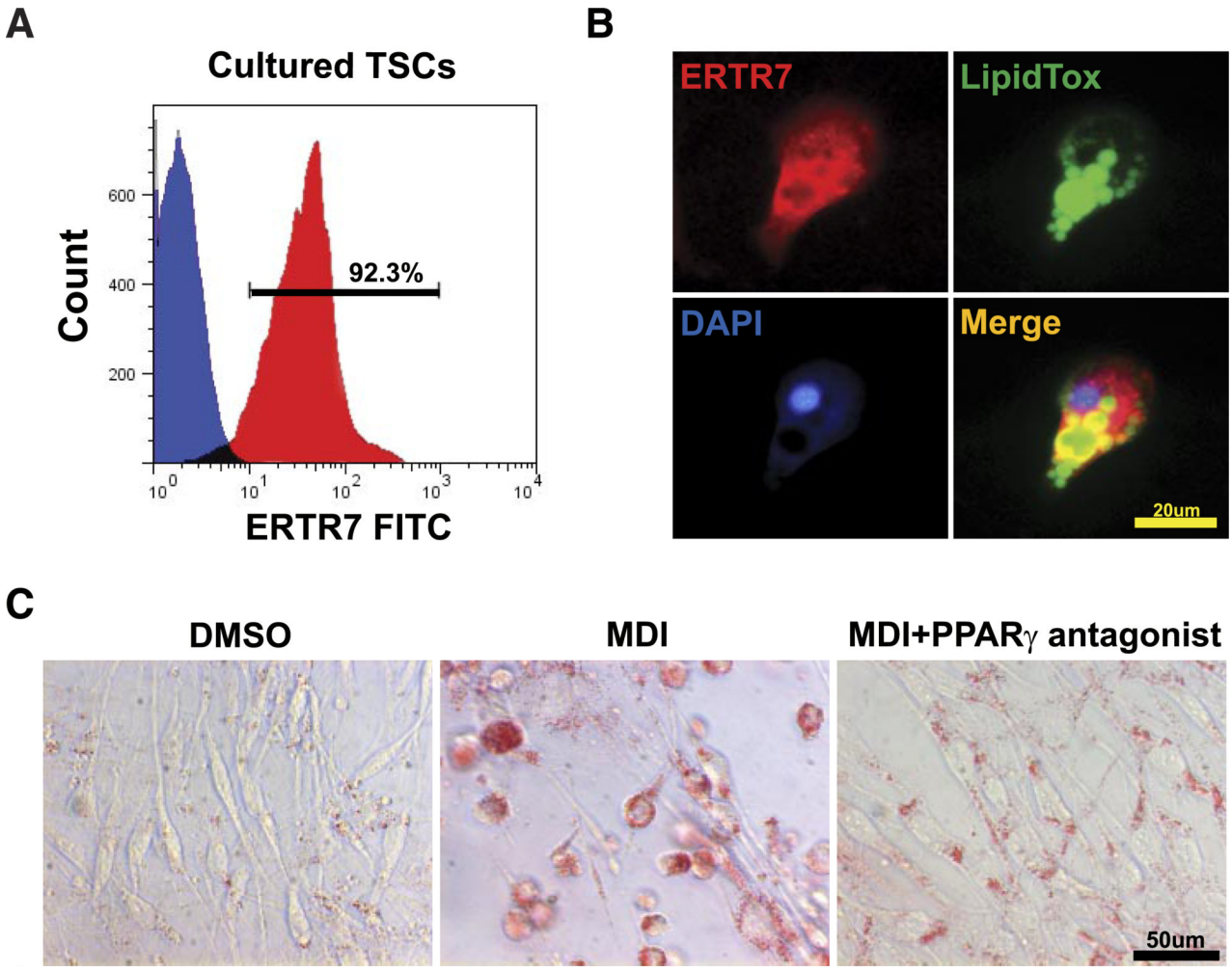

FIGURE 4.

Thymic stromal cells differentiate into adipocyte in vitro. *A*, Most TSCs expressed the fibroblast marker ERTR7. The FACS analysis of cultured TSCs is shown: the negative control cell (blue) did not display specific ERTR7 staining, while most cells (red) expressed ERTR7$^+$. Results are representative of three separate experiments. *B*, Confocal immunofluorescence analysis of cultured TSCs stained for ERTR7 (Alexa Fluor-594), neutral lipids (LipidTOX Green), and DAPI (blue). A number of TSCs contained multilocular lipid droplets characteristic of adipocytes. *C*, The Oil Red O staining (labeled red for neutral lipids) of TSCs from 6-wk-old mice shows a marked change in morphology to round lipid-bearing adipocytes. while PPARγ antagonist (GW9662, 10 μM) inhibits lipid accumulation and adipogenesis.

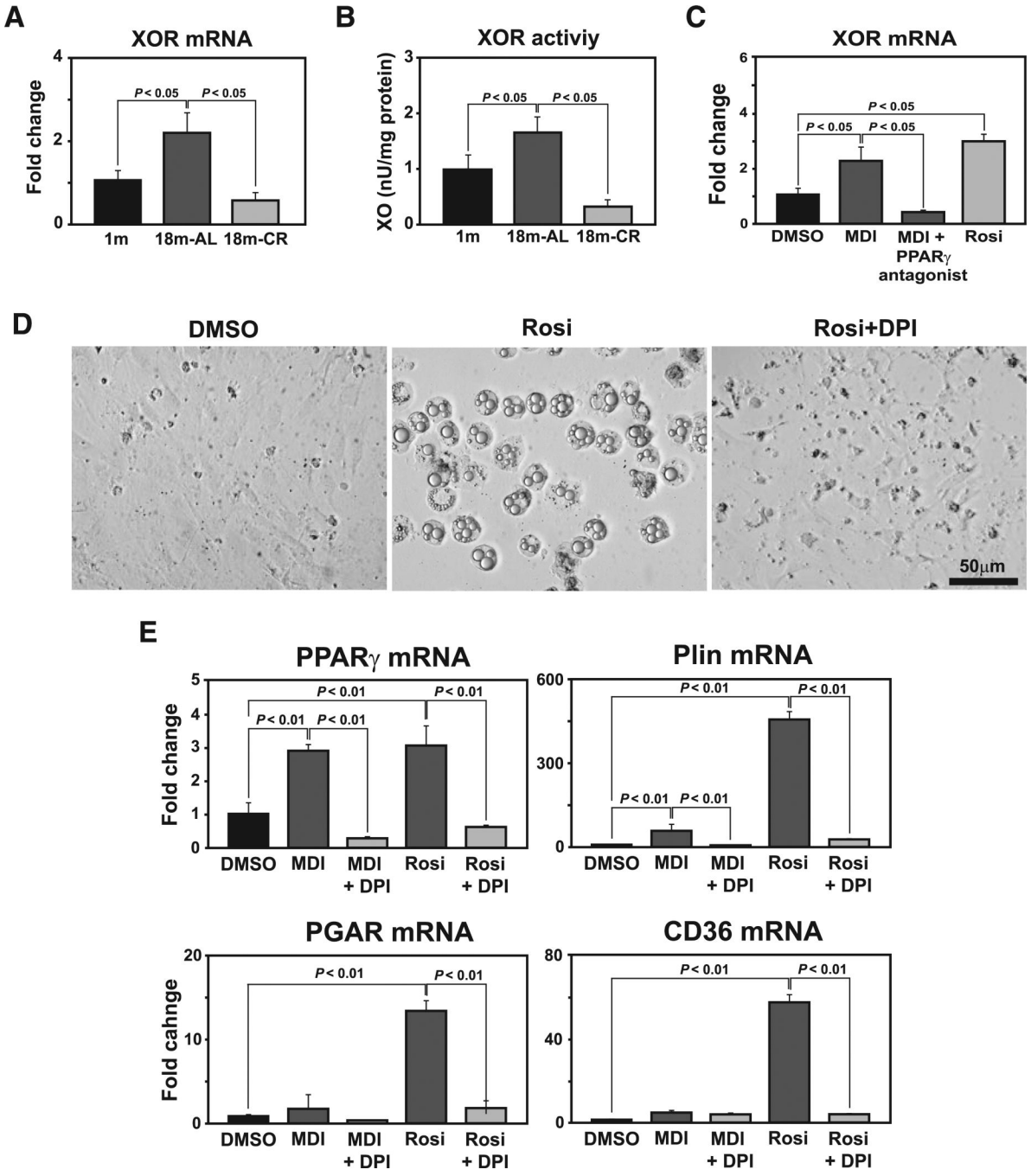

FIGURE 5.

Xanthine oxidoreductase regulates PPAR*γ* expression in TSCs. *A*, Thymic XOR mRNA expression was quantified by real-time PCR analysis (*n* = 6/group). *B*, Total thymic protein was equalized and analyzed for XOR activity. CR prevents the age-related increase in XOR activity in the thymus (*n* = 6/group). *C*, The TSCs (from 3-mo-old mice) were treated with adipogenic cocktail (MDI), rosiglitazone, and MDI together with PPAR*γ* antagonist (GW9662. 1 *μ*M). Compared with vehicle (DMSO)-treated cells, activation of PPAR*γ* up-regulates XOR mRNA. *D*, XOR inhibitor diphenyleneiodonium (DPI; 100 nM) blocks rosiglitazone-mediated adipogenesis of TSCs. *E*, Quantitation of PPAR*γ*, perilipin, PPAR*γ* angiopoietin related (PGAR), and CD36 mRNA expression by real-time PCR demonstrates that XOR inhibitor

(DPI) blocks MDI and rosiglitazone-mediated adipogenesis in TSCs. These data are expressed as means ± SEM and are representative of duplicate wells from three separate experiments.

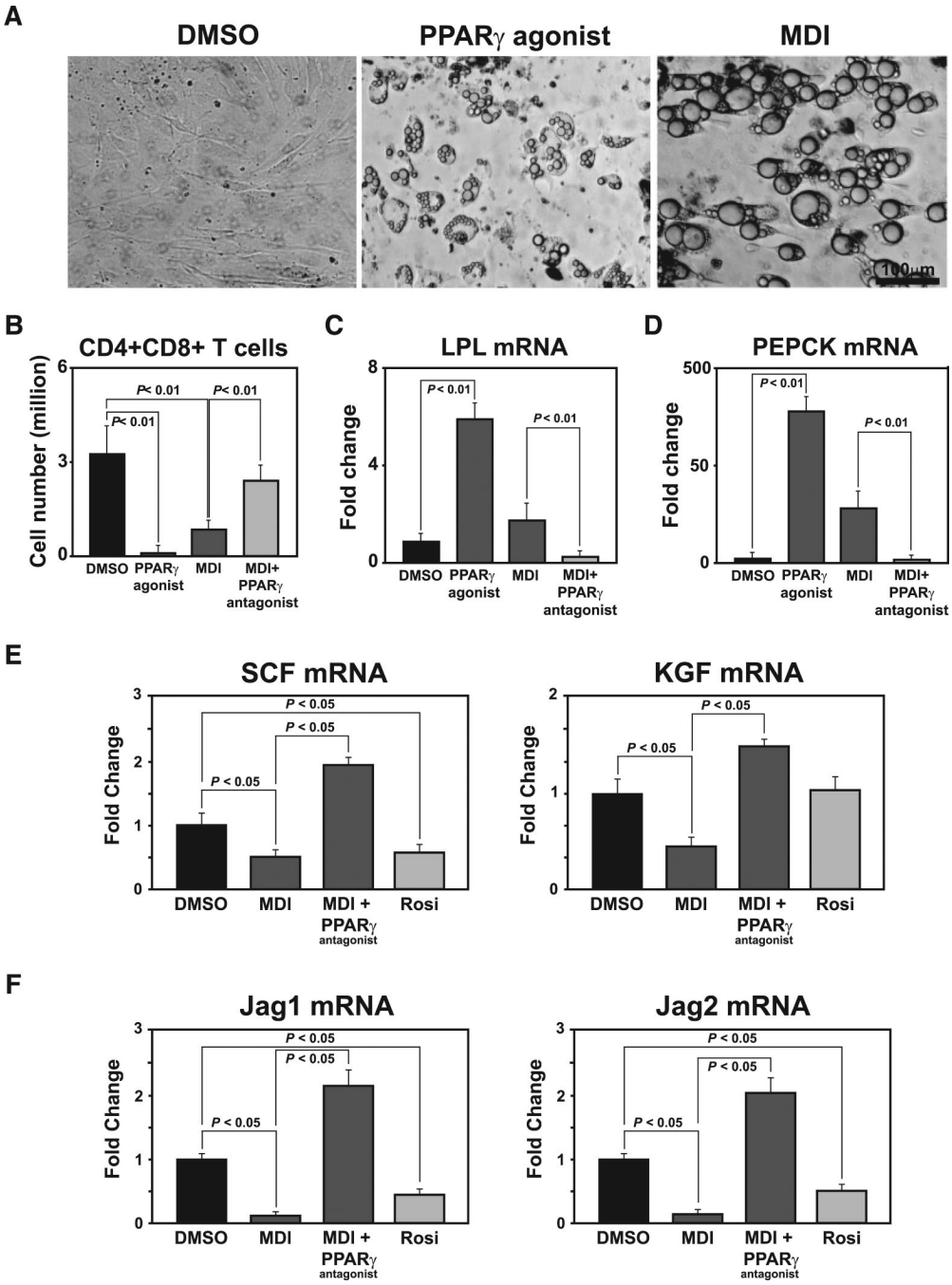

FIGURE 6.

Adipogenesis of stromal cells compromises their T cell development capacity in a PPARγ-dependent pathway. *A*, The OP9-DL1 cells acquire adipocyte morphology upon 1 wk of treatment with rosiglitazone and MDI. *B*, The OP9-DL1 cells were treated with vehicle, rosiglitazone, MDI, and MDI along with PPARγ antagonist GW9662 (1 μM) for 1 wk. The adipogenic media was then replaced and OP9-DL1 stromal cells were cocultured with LSKs for 18 days with IL-7 and Flt3 ligand. The suspension cells were stained with CD4 FITC and CD8-PE and used for FACS analysis. *C*, mRNA expression of lipoprotein lipase (LPL) and (*D*) phosphoenolpyruvate carboxykinase (PEPCK), the PPAR-γ target genes, in OP9-DL1 cells was analyzed by real-time PCR. *E* and *F*, The real-time PCR analysis of stem cell factor (SCF),

keratinocyte growth factor (KGF), Jag1, and Jag2 in OP9-DL1 cells induced to undergo adipogenesis in response to PPARγ agonist and adipogenic cocktail (MDI). MDI treatment in presence of the PPARγ-specific antagonist GW9662 blocks the loss of genes supporting T cell development. All experiments were performed in duplicate wells and repeated thrice. These data are expressed as means ± SEM.

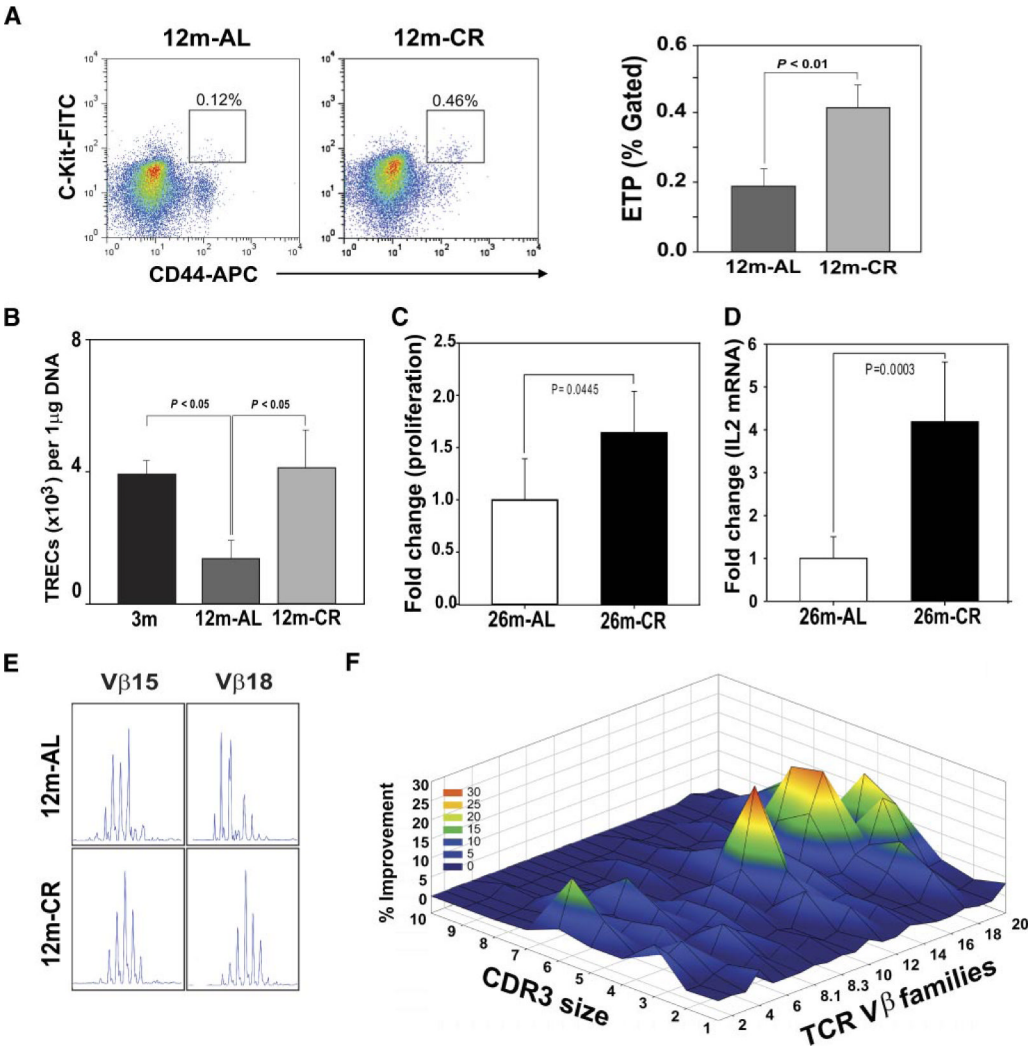

FIGURE 7.

CR-induced inhibition of thymoadipogenesis is associated with increase in thymic output and prevents age-related TCR repertoire restriction. *A*, The ETP ($Lin^{-}CD44^{+}c\text{-}Kit^{high}$) cells in thymus were identified by acquiring 1×10^6 total events, and analysis was performed using CellQuest software on a FACSAria ($n = 5$/group). FlowJo software was utilized for postacquisition compensation and analysis. *B*, The splenic $CD4^+$ T cells were isolated to prepare the DNA, and TREC levels were analyzed using quantitiative PCR analysis. A total of six to eight mice per group were utilized for signal-joint TREC assay and the data are expressed as means ± SEM. The CD4 cells from 26-mo-old mice were stimulated with plate-bound anti-CD3 and anti-CD28 Abs, and (*C*) cell proliferation was analyzed using MTT assay and (*D*) IL-2 mRNA by real-time PCR ($n = 6$/group). *E*, Representative skewed TCR Vβ profile in aged mouse and polyclonal Gaussian distribution of CDR3 lengths in CR. The data were generated using an ABI 3100 sequencer and analyzed using GeneMapper. *F*, The Gaussian distribution profiles were translated into probability distributions as functions of the area under the curve for each CDR3 length. The average distribution of the $CD4^+$ repertoire from 10-mo-old AL fed controls is compared with the CR mice. The statistical quantitation of the CDR3 size of all the TCR Vβ between control and CR mice was performed using CDR3QAssay software. The extent of the change in the CDR3 size distribution is defined as percentage improvement (distance from the mean value). The percentage improvement >3 SDs in the

fragment length of each family indicates that there are significant changes in the Vβ family. These improvements in TCR diversity are represented as landscape surfaces, in which smooth (blue) landscapes represent an unchanged TCR repertoire (diversity). The peaks (in green, yellow, and orange) depict improved amplified peaks of CDR3 lengths. Each line crossing the *y*-axis of the landscape denotes improvement for a specific CDR3 length or size (*x*-axis) of a particular Vβ family (*z*-axis).

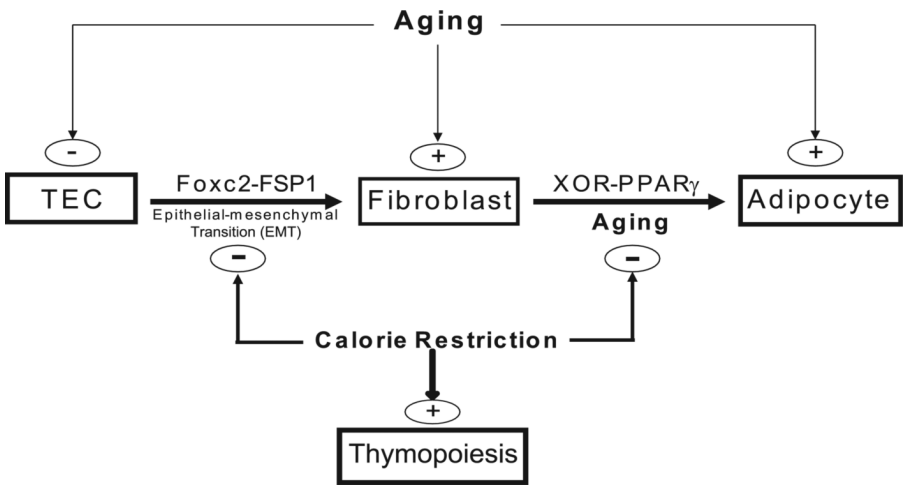

FIGURE 8.

Hypothetical model of mechanism of the action of CR in regulating age-related thymic adiposity. A subset of TECs undergoes EMT and gives rise to a fibroblast population within thymus that can further differentiate into adipocyte via XOR- and PPARγ-dependent mechanisms. CR maintains a thymic stromal microenvironment by inhibiting EMT and age-related increase in XOR- and PPARγ-dependent adipogenesis of EMT-derived fibroblasts.

Table I

Sequences of real-time PCR primer pairs

Gene	Forward (5′ → 3′)	Reverse (5′ → 3′)
GAPDH	TTGATGGCAACAATCTCCAC	CGTCCCGTAGACAAAATGGT
EVA	GGCTGGCTTTCCCTGATGTAT	TTAACCGAACATCTGTCCCGT
Aire	GGTTCTGTTGGACTCTGCCCTG	TGTGCCACGACGGAGGTGAG
IL-7	GGGAGTGATTATGGGTGGTGAG	TGCGGGAGGTGGGTGTAG
KGF	TTGACAAACGAGGCAAAGTG	CCCTTTGATTGCCACAATTC
CXCL12	CAGTGACGGTAAACCAG	ATATGCTATGGCGGAGT
CCL25	TTTGAAGACTGCTGCCTGG	GTCTTCTTCCTAACAAGCC
PPARγ	ACAAGACTACCCTTTACTGAAATTACCAT	TGCGAGTGGTCTTCCATCAC
aP2	GCGTGGAATTCGATGAAATCA	CCCGCCATCTAGGGTTATGA
Perilipin	GACACCACCTGCATGGCT	TGAAGCAGGGCCACTCTC
PGAR	GGAAAAGTCCACTGTGCCTC	AAGATGACCCAGCTCATTGG
CD36	CCTGCAAATGTCAGAGGAAA	GCGACATGATTAATGGCACA
PEPCK	AACTGTTGGCTGGCTCTC	GAACCTGGCGTTGAATGC
XOR	GGTTGTTTCCACTTCCTCCA	TTCCAAGGAAACCTCTGTCG
LPL	TGTGTCTTCAGGGGTCCTTAG	TTTGGCTCCAGAGTTTGACC
IL-2	CGCAGAGGTCCAAGTTCATC	AACTCCCCAGGATGCTCAC